Homocoupling defects in porphyrinoid small molecules and their effect on organic solar cell performance

Peer-reviewed author version

KELCHTERMANS, Mathias; DECKERS, Jasper; BREBELS, Jeroen; KESTERS, Jurgen; VERSTAPPEN, Pieter; THIRUVALLUR EACHAMBADI, Ragha; Liu, Zhen; Van den Brande, Niko; MANCA, Jean; LUTSEN, Laurence; VANDERZANDE, Dirk & MAES, Wouter (2019) Homocoupling defects in porphyrinoid small molecules and their effect on organic solar cell performance. In: Organic Electronics, 69, p. 48-55.

DOI: 10.1016/j.orgel.2019.03.012
Handle: http://hdl.handle.net/1942/28228

Accepted Manuscript

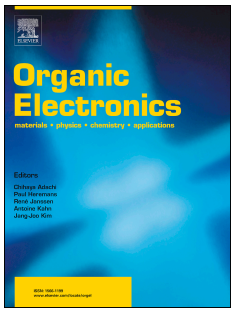

Homocoupling defects in porphyrinoid small molecules and their effect on organic solar cell performance

Mathias Kelchtermans, Jasper Deckers, Jeroen Brebels, Jurgen Kesters, Pieter Verstappen, Raghavendran Thiruvallur Eachambadi, Zhen Liu, Niko Van den Brande, Jean Manca, Laurence Lutsen, Dirk Vanderzande, Wouter Maes

PII: S1566-1199(19)30113-2

DOI: https://doi.org/10.1016/j.orgel.2019.03.012

Reference: ORGELE 5150

To appear in: *Organic Electronics*

Received Date: 17 November 2018

Revised Date: 13 February 2019

Accepted Date: 7 March 2019

Please cite this article as: M. Kelchtermans, J. Deckers, J. Brebels, J. Kesters, P. Verstappen, R.T. Eachambadi, Z. Liu, N. Van den Brande, J. Manca, L. Lutsen, D. Vanderzande, W. Maes, Homocoupling defects in porphyrinoid small molecules and their effect on organic solar cell performance, *Organic Electronics* (2019), doi: https://doi.org/10.1016/j.orgel.2019.03.012.

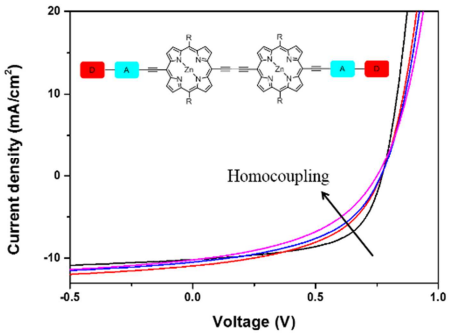

Homocoupling defects in porphyrinoid small molecules and their effect on organic solar cell performance

Mathias Kelchtermans,[a] Jasper Deckers,[a] Jeroen Brebels,[a] Jurgen Kesters,[a] Pieter Verstappen,[a] Raghavendran Thiruvallur Eachambadi,[b] Zhen Liu,[c] Niko Van den Brande,[c] Jean Manca,[b] Laurence Lutsen,[d] Dirk Vanderzande,[a,d] and Wouter Maes[a,d]*

(a) UHasselt – Hasselt University, Institute for Materials Research (IMO), Design & Synthesis of Organic Semiconductors (DSOS), Agoralaan, 3590 Diepenbeek, Belgium

(b) UHasselt – Hasselt University, X-LAB, Agoralaan, 3590 Diepenbeek, Belgium

(c) Physical Chemistry and Polymer Science (FYSC), Vrije Universiteit Brussel, Pleinlaan 2, 1050 Brussels, Belgium

(d) IMEC, Associated lab IMOMEC, Wetenschapspark 1, 3590 Diepenbeek, Belgium

Corresponding author: Tel.: +32 11268312; E-mail: wouter.maes@uhasselt.be

ABSTRACT

Porphyrinoid small molecules can be used as electron donor or acceptor components in bulk heterojunction organic solar cells, which has resulted in steadily improving power conversion efficiencies. However, the effect of material purity is often neglected. In this work, a series of D1-A-π-D2-π-A-D1 conjugated chromophores based on the A_2B_2-*meso*-ethynylporphyrin core is synthesized. Different electron-donating (D1) end groups are chosen to investigate their influence on the material properties and optoelectronic characteristics. The porphyrin small molecules are tested as electron donor materials in bulk heterojunction organic solar cells in combination with $PC_{71}BM$, affording an efficiency up to 4.6% under standard illumination. Furthermore, it is shown that (Glaser type) homocoupled side products are generated during the final Sonogashira cross-coupling reactions, which can be very challenging to remove, and their presence reduces solar cell performance by affecting the open-circuit voltage and fill factor.

KEYWORDS

porphyrins, conjugated small molecules, organic photovoltaics, material purity, homocoupling, Glaser

1. INTRODUCTION

Sustainable energy production remains one of the most significant challenges of modern society. A vital step was taken by the industrial and domestic commissioning of silicon-based solar cells. Nonetheless, their rigidity and considerable production costs are important drawbacks, demanding for alternative and/or complementary solar energy technologies. Solution-processed bulk heterojunction organic photovoltaics (BHJ OPVs) can be applied alongside classical solar cells, showing distinct advantages in terms of flexibility (enabling roll-to-roll processing) and semi-transparency, which allow (among others) for designer textile applications and window integration (building-integrated photovoltaics).[1-5] Small molecule BHJ organic solar cells have gained particular attention over the last decade, owing to the well-defined molecular structure of the donor type small molecules, easy functionalization and reduced batch-to-batch variations as compared to their polymeric counterparts.[6,7] Deviating solar cell results using polymer donor materials have traditionally been attributed to varying polymer molar masses and dispersities, inherent to the uncontrolled cross-coupling polymerization protocols used to prepare these materials.[8-10] Moreover, homocoupling 'defect' structures have recently been identified as one of the plausible causes for batch-to-batch variations when using state of the art push-pull type conjugated polymers.[11-15] Although homocoupling side reactions also occur upon performing Pd-catalyzed cross-coupling reactions in the final stages of small molecule syntheses, and their negative impact on solar cell performance has been reported,[16,17] these byproducts are often readily removed upon purification, thereby reducing their importance for small molecule BHJ OPVs. Nevertheless, it was shown before that it is not always trivial to fully eliminate homocoupled impurities.[16]

Inspired by the natural photosynthetic antenna systems, porphyrinoid chromophores have always been attractive candidates for solar light to energy conversion. They possess some

intrinsic properties beneficial for electronic applications, such as distinct absorptions in both the high and low wavelength region of the solar spectrum with reasonably high absorption coefficients, high thermal stability and a large π-conjugated system allowing for strong intermolecular interactions. Additionally, the straightforward modification of the porphyrin periphery (*meso*- and β-positions) and central core (through metalation) greatly influences their photo- and electrochemistry. Earlier success stories in the field of dye-sensitized solar cells[18,19] have motivated researchers to implement similar materials in BHJ OPVs. Most commonly, *meso*-ethynyl substituted push-pull porphyrin derivatives are used, wherein the electron-rich porphyrin core is surrounded by two solubilizing aromatic units and two ethynyl moieties that prevent out-of-plane twisting to ensure a fully conjugated system.[20-22] In the last couple of years, strong efforts were made to incorporate porphyrin derivatives as electron donor type materials in BHJ organic solar cells, resulting in outstanding power conversion efficiencies (PCEs) up to 9%.[23-26] These promising results inspired other researchers to fabricate ternary devices using a porphyrin and a polymer or two porphyrins as donor materials and $PC_{71}BM$ ([6,6]-phenyl-C_{71} butyric acid methyl ester) as acceptor, leading to record efficiencies around 11%.[27,28] Porphyrin-based acceptor materials, on the other hand, showed rather disappointing results until Li *et al*. reported a porphyrin bearing four perylene diimide units affording an efficiency of 7.4% in combination with the donor polymer PBDB-T.[29] Despite the impressive leap forward, the best is likely still to come for porphyrin-based OPVs, for instance in combination with the novel generations of non-fullerene acceptors,[30-33] and continuous research efforts on novel materials and devices are hence still very useful.

In the presented work, a number of advanced porphyrinoid materials with a donor-acceptor-π-porphyrin(donor)-π-acceptor-donor (D1-A-π-D2-π-A-D1) structural motif have been prepared (Figure 1). The benzo[*c*][1,2,5]thiadiazole acceptor unit was combined with four different electron-donating units and coupled to a central zinc-porphyrin via a Sonogashira approach.

The influence of the various electron donor units on the photophysical, electrochemical and photovoltaic features of the porphyrin molecules has been studied. As it was noticed early in this study that homocoupling occurred upon performing the final Sonogashira cross-coupling reactions, this became a particular point of attention. The occurrence and importance of homocoupling for the final device performance was analyzed and suggestions are provided to avoid these defect structures.

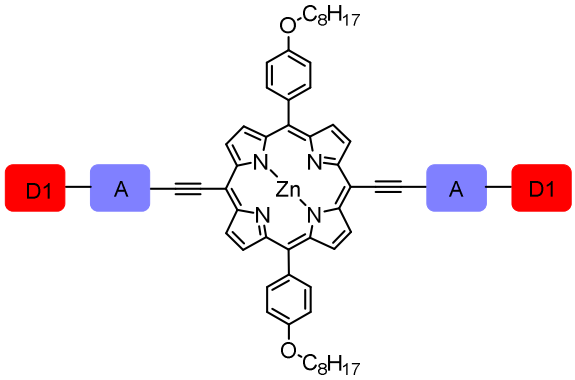

Figure 1. General D1-A-π-D2-π-A-D1 structure of the porphyrin materials studied here.

2. RESULTS AND DISCUSSION

2.1. Material synthesis and characterization

The presented porphyrin small molecules are composed of multiple known building blocks. An alkynated porphyrin core (**Porph**), an electron-deficient benzo[*c*][1,2,5]thiadiazole unit (**BT**) and various electron-donating units (**D**) – i.e. bis(4-hexylphenyl)amine (**DPA**), thiophene (**T**), 4*H*-dithieno[3,2-*b*:2',3'-*d*]pyrrole (**DTP**) and benzo[1,2-*b*:4,5-*b*']dithiophene (**BDT**) – were selected based on their established significance in organic solar cell materials.[34-39] Zinc was chosen as the metal center because of its simple synthetic incorporation, the additional planarization of the molecule and the ability to coordinate to pyridine, allowing morphology optimization of the BHJ photoactive layer.[40,41] The porphyrin core and the various electron-donating subunits were prepared according to literature procedures.[34,39,42-44] In the next step, several cross-coupling reactions were performed

between 4,7-dibromobenzo[*c*][1,2,5]thiadiazole and the (mono-functionalized) electron-donating units (Scheme 1; see SI for experimental details). At first, bis(4-hexylphenyl)amine was used to synthesize **BT-DPA** using a Buchwald-Hartwig reaction. Next, Suzuki cross-coupling with 3-(2-ethylhexyl)thiophene-2-boronic acid pinacol ester was performed to obtain **BT-T**. Finally, 1-(4*H*-dithieno[3,2-*b*:2',3'-*d*]pyrrol-4-yl)-2-hexyldecan-1-one (**DTP**) and 4,8-bis(2-ethylhexyloxy)benzo[1,2-*b*:4,5-*b*']dithiophene (**BDT**) were chosen because of their stronger electron-donating characteristics to further decrease the optical gap of the final small molecules. **BT-DTP** and **BT-BDT** were prepared by Stille cross-coupling between 4,7-dibromobenzo[*c*][1,2,5]thiadiazole and monostannylated **DTP** or **BDT**, respectively. Moderate yields ranging from 40−60% were observed, customary for mono-cross-couplings due to formation of undesirable bis-substituted products. For **BT-DTP**, a higher yield of 81% was observed due to the addition of a two-fold excess of 4,7-dibromobenzo[*c*][1,2,5]thiadiazole.

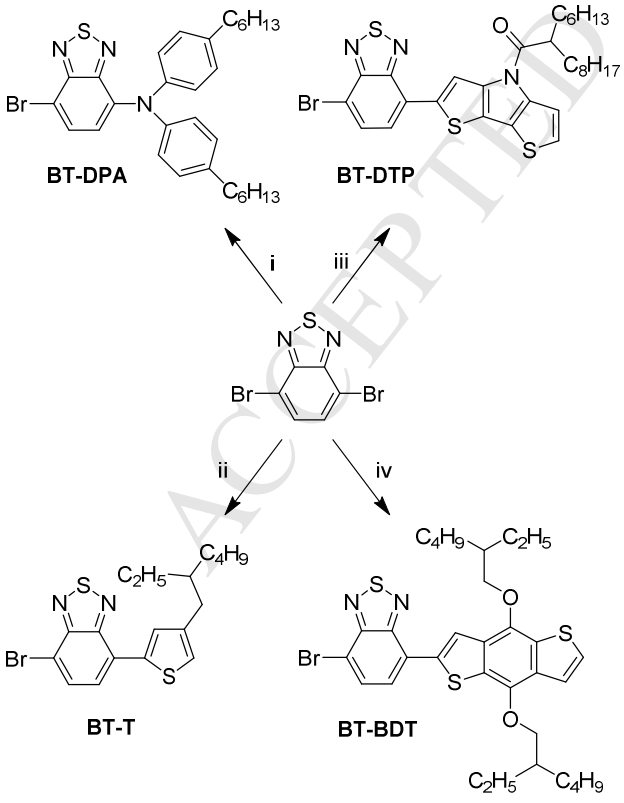

Scheme 1. BT-D synthesis: i) bis(4-hexylphenyl)amine, P(*t*-Bu)$_3$, NaO*t*-Bu, Pd(OAc)$_2$, toluene, 100 °C, 20 h (43%); ii) 3-(2-ethylhexyl)thiophene-2-boronic acid pinacol ester, Na_2CO_3 (aq, 2M), Aliquat366, $Pd(PPh_3)_2Cl_2$, toluene, 70 °C, 20 h (48%); iii) 2-hexyl-1-(2-(trimethylstannyl)-4*H*-dithieno[3,2-*b*:2',3'-*d*]pyrrol-4-yl)decan-1-one, $Pd(PPh_3)_4$, toluene, 100 °C, 20 h (81%). iv) (4,8-bis(2-ethylhexyloxy)benzo[1,2-*b*:4,5-*b*']dithiophen-2-yl)trimethylstannane, $Pd(PPh_3)_4$, toluene, 80 °C, 20 h (55%).

Particular attention was then devoted to the preparation of the final small molecules by Sonogashira cross-coupling between the A_2B_2-*meso*-ethynylporphyrin core (**Porph**) and the monobrominated push-pull moieties (Scheme 2). The reaction conditions were initially optimized for **Porph-BT-DPA** (Table S1). This molecule was obtained in a reasonably good yield of 70% upon using $Pd_2(dba)_3$ as a catalyst and PPh_3 as ligand in tetrahydrofuran, whereas much lower yields (around 30%) were achieved for $Pd(PPh_3)_4$ in toluene or $Pd_2(dba)_3/AsPh_3$ in tetrahydrofuran. The optimal reaction conditions were then applied to the other porphyrinoid small molecules, resulting in overall good yields, except for **Porph-BT-T**, which only gave a yield of 25% under the same conditions. Changing the solvent system to toluene:DMF (3:1) increased the yield to 67%. The final materials were unambiguously characterized by ^{1}H NMR spectroscopy and high resolution mass spectrometry.

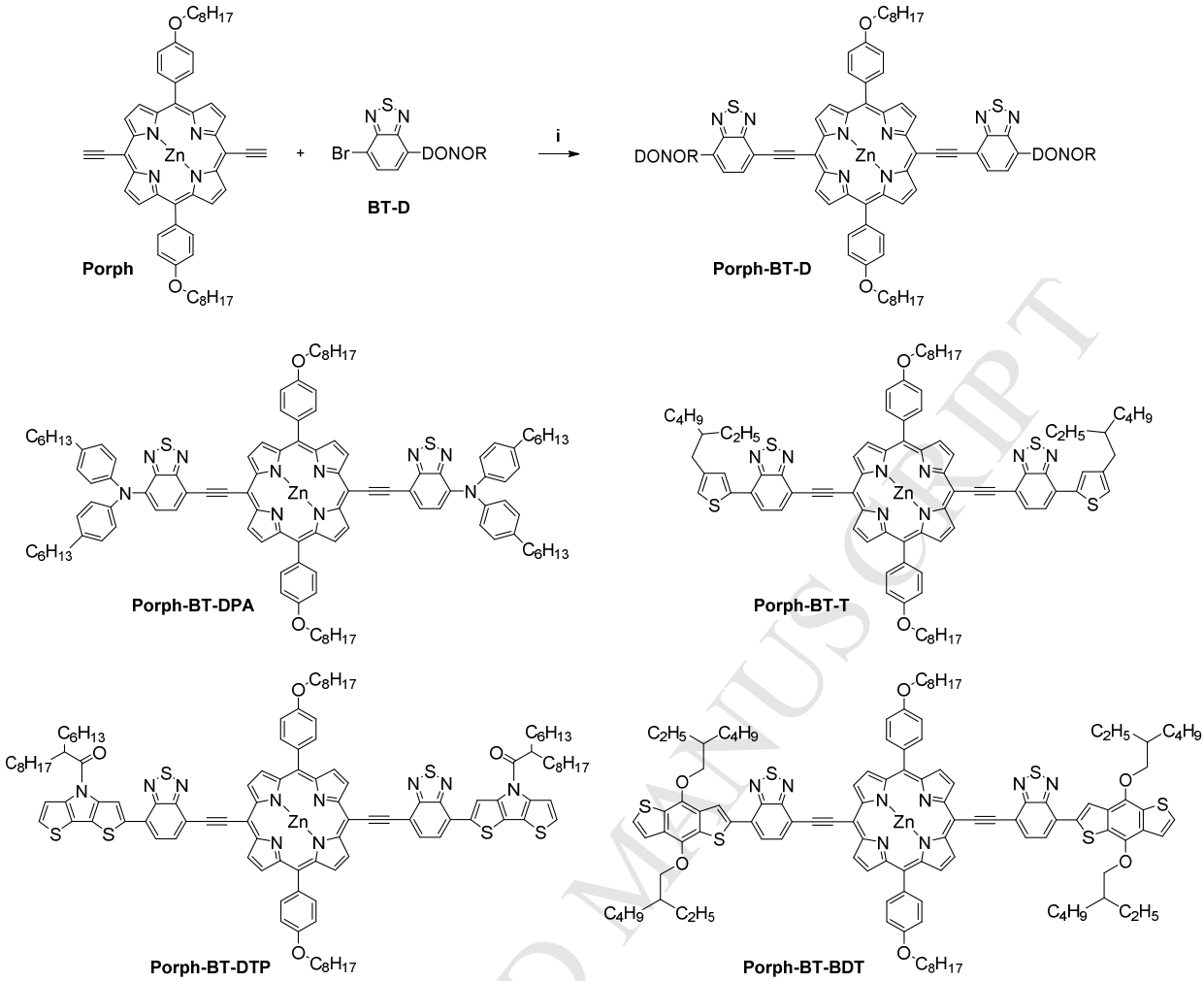

Scheme 2. Porph-BT-D synthesis: i) $Pd_2(dba)_3$, PPh_3, CuI, THF (toluene/DMF for **BT-T**), Et_3N, 50 °C, 20 h; **Porph-BT-DPA** (70%), **Porph-BT-T** (67%), **Porph-BT-DTP** (75%), **Porph-BT-BDT** (75%).

Because of the limited solubility of the final porphyrinoid molecules and the similar polarity of certain impurities, purification was not straightforward and great care had to be taken to get rid of undesirable (trace) impurities. For **Porph-BT-BDT**, after several silica gel column chromatography runs using different eluents, size exclusion chromatography (using Bio-Beads) and precipitation, the impurity that eluted almost alongside the target molecule was identified by MALDI-TOF (Matrix-Assisted Laser Desorption/Ionization-Time of Flight) mass spectrometry as the homocoupled product **$(Porph)_2$-BT-BDT**, featuring two central diethynyl-linked porphyrin units (Figure 2). This type of homocoupling (Glaser coupling),

which occurs in standard Sonogashira cross-couplings due to the presence of oxygen, is far from unknown and has mostly been researched for synthetic purposes.[45-48] Nonetheless, it has not been discussed yet in the field of porphyrinoid OPV materials – except for a short note in the SI[49] – and the effect of its presence on solar cell performance has not been investigated so far (although a purposely developed 'dimeric' porphyrin was studied before[50]). Using the aforementioned purification steps (repetitive silica gel column and size exclusion chromatography), analytically pure **Porph-BT-BDT** was obtained and **(Porph)$_2$-BT-BDT** was isolated in a ratio up to 10 wt%. Low amounts of homocoupling were also found in the reaction mixtures of other porphyrin small molecules (see Figure S5-S6), but they were not isolated.

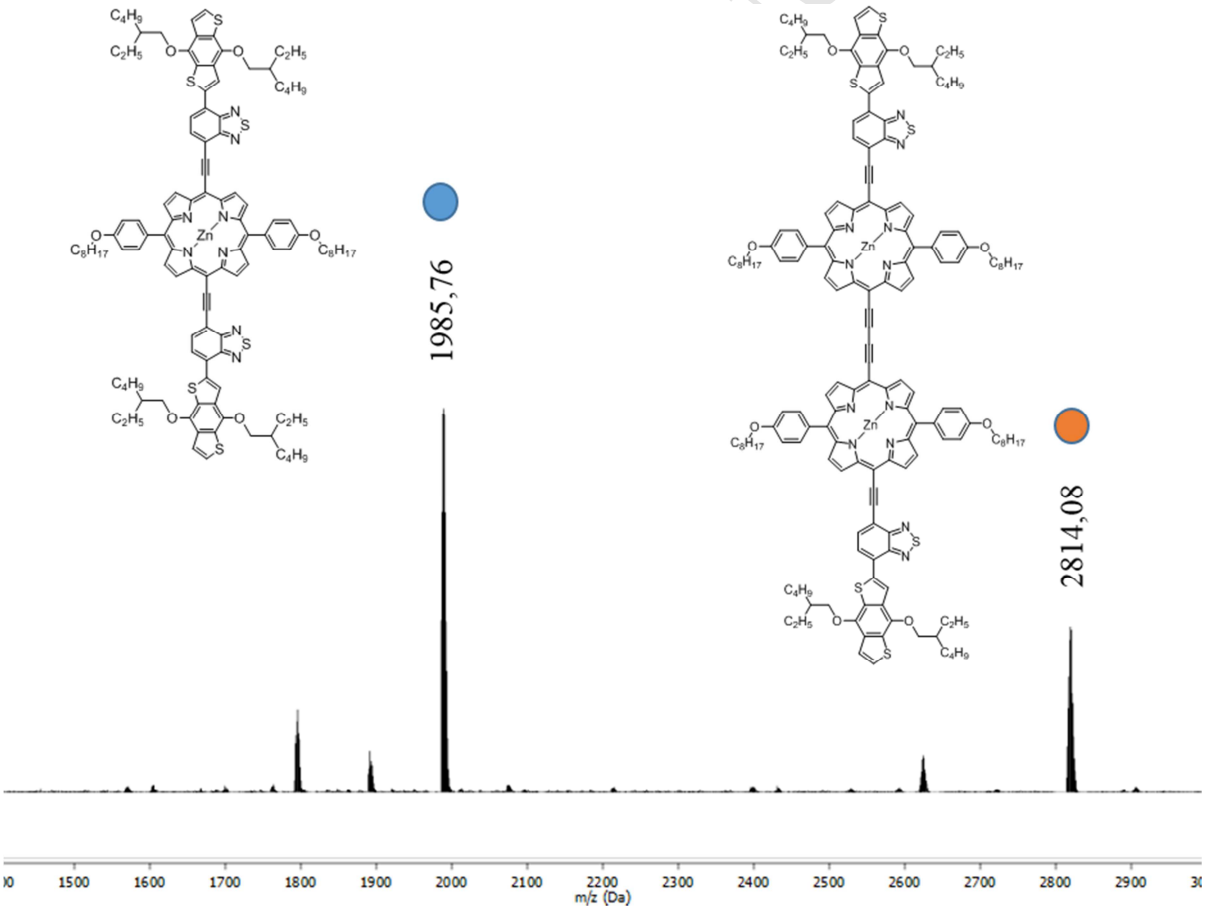

Figure 2. MALDI-TOF mass spectrum of **Porph-BT-BDT** after purification by silica gel column chromatography, showing the presence of the homocoupled byproduct **(Porph)$_2$-BT-BDT**.

Such a tedious purification method is obviously undesirable, considering time and cost effectiveness. Therefore, the alkyne and bromine functionalities were interchanged with the aim to simplify material purification (Scheme 3). Although Glaser coupling is not eliminated under these conditions, it will occur between two **BT-BDT-alkyne** units instead of two porphyrin cores. Eventually, the same product, **Porph-BT-BDT**, was obtained without the formation of **(Porph)$_2$-BT-BDT**.

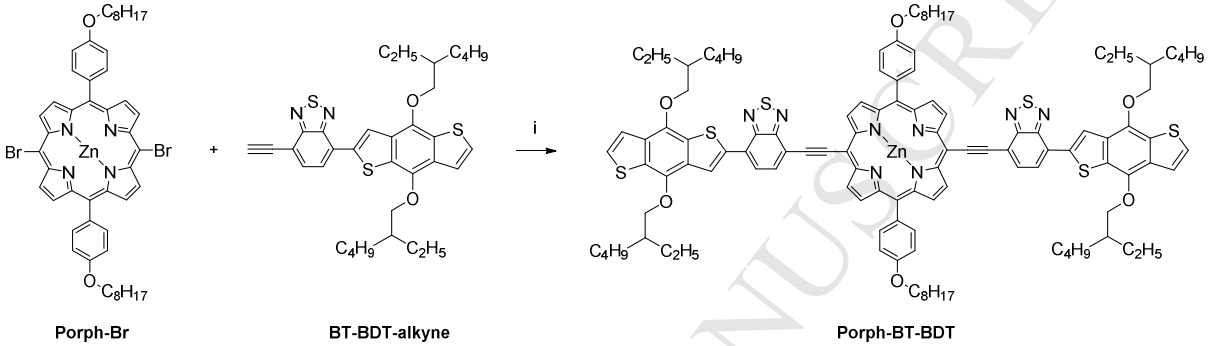

Scheme 3. Porph-BT-BDT synthesis using interchanged functionalities: i) $Pd_2(dba)_3$, PPh_3, CuI, THF, Et_3N, 50 °C, 20 h (35%).

Thermogravimetric analysis (TGA) and rapid heat-cool calorimetry (RHC) were performed to investigate the thermal properties of the porphyrin chromophores (Figure S7-S8). TGA showed that the porphyrins are thermally stable (with respect to mass loss) up to 300 °C. RHC analysis, using heating and cooling rates of 500 K.min^{-1}, indicated that **Porph-BT-DPA** and **Porph-BT-T** show a melting trajectory, whereas no clear thermal transitions can be seen for **Porph-BT-DTP** and **Porph-BT-BDT** in the temperature interval studied.

Absorption spectra of the porphyrin small molecules in solution and thin film are shown in Figure 3. Two distinct, similarly intense absorption regions can be observed. The region between 400 and 600 nm stems from the porphyrin Soret band (S_0 to S_2 transition) and the **BT-D** end groups, while the region between 600 and 850 nm originates from intramolecular charge transfer between the porphyrin core and the **BT-D** push-pull moieties, driving the

absorption to the near-infrared (NIR) region.[51] Additionally, this driving force is connected to the electron-donating capabilities of the donor end groups. Upon going from solution to thin film, the porphyrinoid molecules exhibit a bathochromic shift of ~50 nm and an additional absorption shoulder in the NIR, indicating strong π-π intermolecular interactions. The optical gaps (E_g^{opt}), estimated from the absorption edges in film, range from 1.5 to 1.6 eV (Table 1).

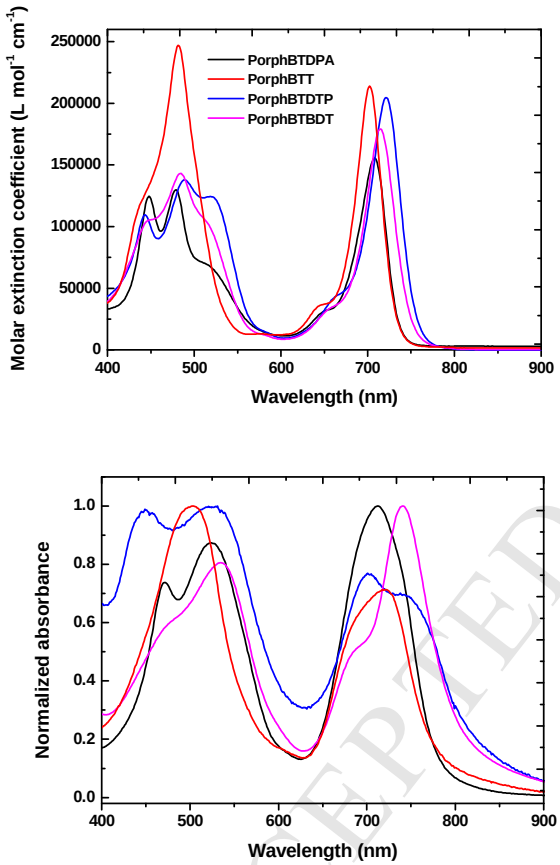

Figure 3. UV-Vis absorption spectra of the **Porph-BT-D** molecules in THF solution (top) and thin film (bottom).

Electrochemical material properties were investigated by cyclic voltammetry (CV; Table 1). The HOMO (highest occupied molecular orbital) energy levels are found between −5.53 and −5.08 eV, and differ due to the varying electron-donating capabilities of the donor moieties. The corresponding LUMO (lowest unoccupied molecular orbital) levels are located between

−3.52 and −3.54 eV. This results in LUMO-LUMO offsets of ~0.4 eV compared to $PC_{71}BM$ (LUMO = −3.91 eV under the same conditions), which allows efficient porphyrin to fullerene electron transfer. For the homocoupled species **(Porph)$_2$-BT-BDT**, HOMO and LUMO energy levels of −5.29 and −3.77 eV, respectively, were obtained.

Table 1. Optical and electrochemical data for the **Porph-BT-D** molecules.

Porph-BT-D	$\lambda_{max\ film}$[a]/ **nm**	**Log** ε_{max}[b]/ **L mol^{-1} cm^{-1}**	$E_{g\ film}$[c]/ **eV**	E_{ox}[d]/ **eV**	E_{red}[d]/ **eV**	$E_{g\ cv}$[e]/ **eV**	E_{HOMO}[f]/ **eV**	E_{LUMO}[f]/ **eV**
Porph-BT-DPA	712	5.192	1.60	0.37	−1.44	1.81	−5.33	−3.52
Porph-BT-T	702	5.330	1.60	0.12	−1.42	1.53	−5.08	−3.54
Porph-BT-DTP	720	5.311	1.52	0.32	−1.43	1.75	−5.28	−3.53
Porph-BT-BDT	740	5.253	1.54	0.57	−1.43	2.00	−5.53	−3.53
(Porph)$_2$-BT-BDT	694	/	1.34	0.38	−1.13	1.51	−5.29	−3.77

[a] Wavelength of maximum absorption at the low energy side of the spectrum. Films were prepared by drop-casting a solution of the porphyrin material onto a quartz disc. [b] Absorption coefficient (in THF solution) of the absorption peak at the higher wavelength side. [c] Optical gap, determined by the onset of the solid-state UV-Vis-NIR spectrum. [d] Onset potentials vs. Fc/Fc^+. [e] Electrochemical bandgap. [f] Determined from the onset of oxidation/reduction in cyclic voltammetry.

2.2. Solar cell fabrication and analysis

To investigate the photovoltaic properties of the porphyrin series, solution-processed BHJ organic solar cells were fabricated using the **Porph-BT-D** materials as electron donors and $PC_{71}BM$ as the electron acceptor in a traditional device architecture ITO/PEDOT:PSS/**Porph-BT-D**:$PC_{71}BM$/Ca/Al. The photoactive layers were carefully optimized with respect to donor:acceptor ratio, active material and additive concentration and various annealing parameters (Tables S2−S5). *J-V* measurements under illumination were executed using

standard AM1.5G conditions with an intensity of 100 mW cm^{-2} and the results are summarized in Figure 4 (top) and Table 2.

The active layers based on **Porph-BT-DPA**:$PC_{71}BM$, spin-coated from chlorobenzene, gave moderate power conversion efficiencies, with a maximum of 2.1%. The optimal weight ratio of porphyrin to $PC_{71}BM$ was found to be 1:3, whereas increasing the amount of porphyrin lowered the PCE to 1.4%. Pyridine is commonly used as a processing additive to improve film morphologies[52-54] when using Zn(II)-porphyrins due to its capability to coordinate to the metal ion, limiting π-π stacking and thereby modifying the donor-acceptor interface alongside the open-circuit voltage (V_{oc}).[55] However, the addition of 1 vol% pyridine to **Porph-BT-DPA** did not further improve the PCE. For the other three molecules, pyridine was anyway required to increase the solubility. Unfortunately, using various volume concentrations of pyridine (1 to 50 vol%, Tables S3-S4), the PCE for the solar cells based on **Porph-BT-T** and **Porph-BT-DTP** remained very low (around 1.0%; Table 2). Thermal annealing at 110 °C did not positively affect these devices. Finally, the solar cells made from **Porph-BT-BDT** were carefully optimized for pyridine concentration, porphyrin to $PC_{71}BM$ weight ratio and thermal annealing (Table S5). In this case, the *J-V* characteristics gradually improved upon adding more pyridine, with a maximum at 15 vol% pyridine. While increasing the porphyrin to $PC_{71}BM$ weight ratio at first seemed detrimental for the photovoltaic performance, this did lead to enhanced efficiencies upon additional thermal annealing at 110 °C. The strong increase in short-circuit current density (J_{sc}) and fill factor (FF) pushed the (maximum) PCE to 4.6% (Table 2). The external quantum efficiency (EQE) spectrum for this device showed a broad photo response from 300 up to 850 nm (Figure 4, bottom). Modest EQE values ranging from 22 to 44% were observed for the first three devices, with a characteristic dip around 600 nm, whereas the thermally annealed **Porph-BT-BDT** device showed a larger EQE up to 57% in the Soret region.

Table 2. Photovoltaic characteristics of the optimized BHJ organic solar cells based on **Porph-BT-D**:$PC_{71}BM$ blends, processed from chlorobenzene.

Porph-BT-D	Ratio	Pyridine	Annealing	V_{oc} / V	J_{sc} / mA cm^{-2}	FF	PCE[a]
Porph-BT-DPA	1:3	/	/	0.72	7.48	0.39	2.11 (2.00)
Porph-BT-T	1:1	25 vol%	/	0.76	4.35	0.31	1.01 (0.75)
Porph-BT-DTP	1:1	45 vol%	/	0.74	4.57	0.29	0.98 (0.88)
Porph-BT-BDT	2:1	35 vol%	/	0.83	6.65	0.38	2.07 (1.91)
Porph-BT-BDT	2:1	35 vol%	110 °C	0.78	10.19	0.58	4.59 (4.27)

[a] Average efficiencies over at least 3 devices in brackets.

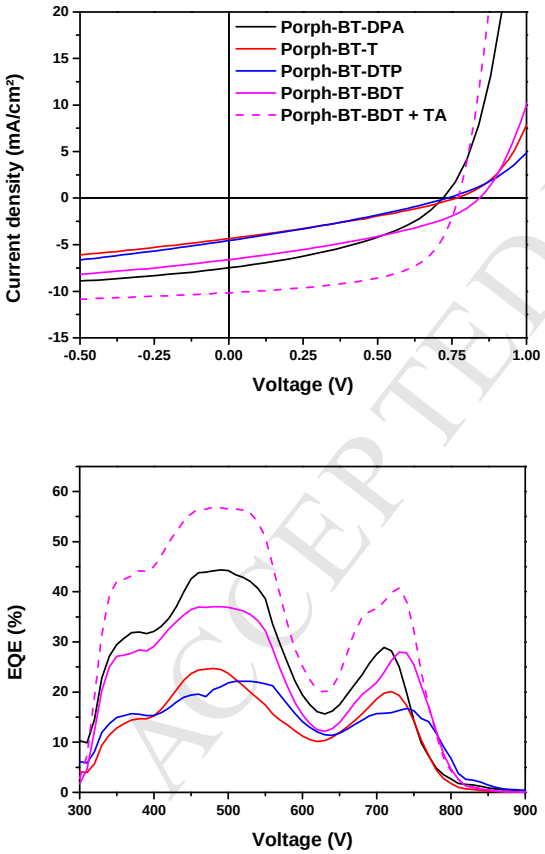

Figure 4. *J-V* characteristics of the optimized solar cell devices prepared from the different **Porph-BT-D**:$PC_{71}BM$ blends (top) and corresponding EQE spectra (bottom).

Single carrier devices were then made to determine the hole mobilities of the **Porph-BT-D**:$PC_{71}BM$ films (Figure S18). A rather good mobility of 1.8 x 10^{-4} cm^2 V^{-1} s^{-1} was obtained for **Porph-BT-DPA**, almost two orders of magnitude larger than the values obtained for **Porph-BT-T** and **Porph-BT-DTP**. This large difference in mobility is also reflected in the J_{sc} of the devices. The hole mobilities for the single carrier devices made from **Porph-BT-BDT** increased from 1.7 x 10^{-5} cm^2 V^{-1} s^{-1} for the as-cast device to 1.9 x 10^{-4} cm^2 V^{-1} s^{-1} after thermal annealing, in line with the significant increase in J_{sc} (from 6.65 to 10.19 mA cm^{-2}).

To gain additional insight into the different performances upon varying the electron-donating units and thermal annealing of the best devices, the morphologies of the active layers were investigated by atomic force microscopy (AFM) (Figure 5). The active layers containing either **Porph-BT-DPA** or **Porph-BT-DTP** displayed intimately mixed morphologies, with some larger particles spread throughout the layer. Intimate mixing generally facilitates the dissociation of photogenerated excitons into free electron and holes but limits charge transport, leading to higher geminate charge recombination rates, which verifies to moderate short-circuit currents and fill factors.[56] The AFM images of the pristine **Porph-BT-T**:$PC_{71}BM$ and especially the **Porph-BT-BDT**:$PC_{71}BM$ active layer exhibited a slightly more coarse phase separation. However, this is not directly reflected in their photovoltaic characteristics. After thermal annealing of the **Porph-BT-BDT**:$PC_{71}BM$ active layer at 110 °C, the phase separation increased further and small fibrillar structures appeared. These ordered features are beneficial for charge transport and may be at the origin of the improved J_{sc} and FF.[57] Furthermore, thermally induced aggregation or ordering is known to yield an increase of the effective HOMO level of the polymer and a corresponding red-shift of the onset of the charge transfer band, and therefore of a reduction of the V_{oc}.[58]

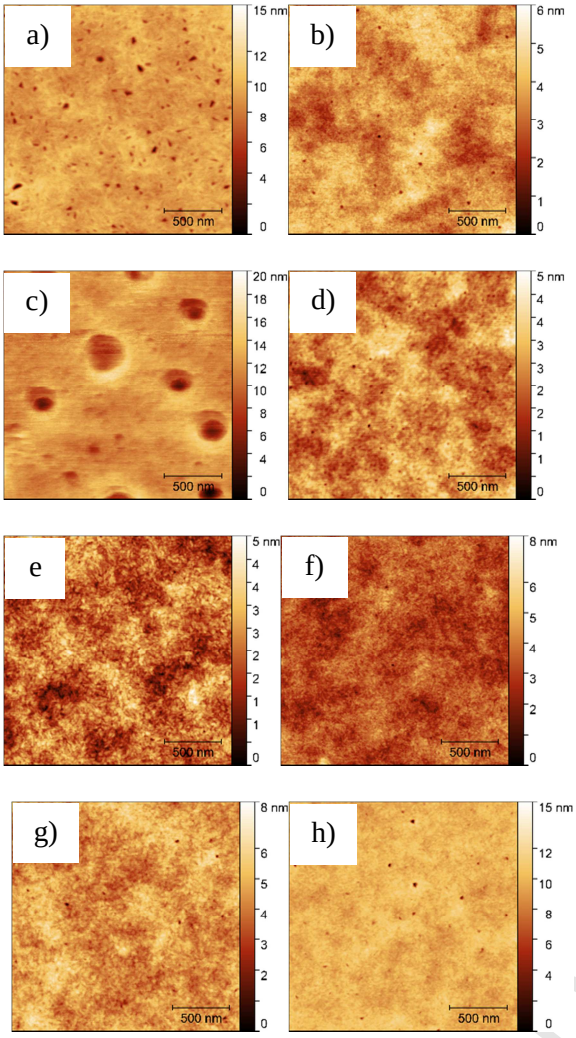

Figure 5. AFM height images (2 µm x 2 µm) of the optimized solar cell devices prepared from a) **Porph-BT-DPA**, b) **Porph-BT-T**, c) **Porph-BT-DTP**, d) **Porph-BT-BDT**, e) **Porph-BT-BDT** with thermal annealing at 110 °C, f) **Porph-BT-BDT** + 1 wt% **(Porph)$_2$-BT-BDT**, g) **Porph-BT-BDT** + 5 wt% **(Porph)$_2$-BT-BDT**, h) **Porph-BT-BDT** + 10 wt% **(Porph)$_2$-BT-BDT**.

The promising device performances during the pyridine optimization for the **Porph-BT-BDT** device led to extensive optimization efforts (Table S5), requiring a lot of material. For this reason, different porphyrin batches were prepared, which were eventually all tested using the optimal processing conditions (Table S6). Remarkably, fairly large differences in photovoltaic performance were observed, going from PCE of 3.6 to 4.6%, for (supposed to be) an identical donor material. As mentioned in the introduction, minor amounts of (homocoupled)

impurities can have a considerable impact on the OPV device characteristics.[14-17] As a consequence, leftover trace amounts of **(Porph)$_2$-BT-BDT** are likely to cause variations in the performance of our devices. To investigate the influence of the presence of the homocoupled side product in a more systematic manner, a series of devices were prepared (using the optimal processing conditions) to which increasing amounts of **(Porph)$_2$-BT-BDT** were added (Table 3, S7, Figure S16-S17). Adding 1 wt% of (**Porph)$_2$-BT-BDT** already had a significant effect on the photovoltaic performance. A large drop in FF was observed, indicating a morphological cause, but also the V_{oc} decreased slightly. Surprisingly, the J_{sc} initially increased slightly. Further increase of the homocoupling content to 5 and 10 wt% reduced the overall PCE to 3.8 and 3.4%, respectively.

Table 3. Photovoltaic characteristics for optimized **Porph-BT-BDT**:$PC_{71}BM$ solar cells (annealed at 110 °C) upon gradual addition of the homocoupled side product **(Porph)$_2$-BT-BDT** to the active layer blend.

(Porph)$_2$-BT-BDT	**V_{oc} / V**	**J_{sc} / mA cm^{-2}**	**FF**	**PCE[a]**
/	0.78	10.19	0.58	4.59 (4.27)
1 wt%	0.76	10.92	0.49	4.08 (3.97)
5 wt%	0.76	10.47	0.48	3.84 (3.80)
10 wt%	0.74	10.21	0.45	3.39 (3.35)

[a] Average efficiencies over at least 3 devices in brackets.

The hole mobility for the optimized blend dropped one order of magnitude after addition of 10 wt% **(Porph)$_2$-BT-BDT**. Surprisingly, the decreased hole mobility did not negatively affect the J_{sc}. This might possibly be related to the intermediate LUMO level of the homocoupled species (Table 1), which then serves as a cascade to facilitate charge transfer to $PC_{71}BM$.[28]

As discussed above, the AFM images of the optimized active layer based on **Porph-BT-BDT** showed the most coarse structure and small fibrillar structures beneficial for charge transport. Upon adding 1% of (**Porph)$_2$-BT-BDT**, the surface morphology already notably changed to a more finely dispersed blend (Figure 5). This trend continues upon further increasing the amount of homocoupling, explaining the gradual drop in fill factor.

3. CONCLUSIONS

In conclusion, four new porphyrin small molecules with a D1-A-π-D2-π-A-D1 built-up were successfully synthesized. The moderately electron-deficient benzothiadiazole moiety was chosen as the acceptor unit in combination with different donor units to provide materials with optical gaps ranging from 1.52 to 1.60 eV in film. Although the studied materials do not show the best solar cell results in the field, the notable (negative) effect of homocoupled side products originating from the applied (Sonogashira) synthetic protocol was disclosed in this work. The emergence of these side products seems to be underestimated so far. Although the present system seems to be rather tolerant to these impurities (as compared to other polymer and small molecule materials previously investigated[14-17]), it remains an important point of attention for future endeavors on porphyrin-based photovoltaic systems. Moreover, it is likely to be of relevance to related fields employing similar materials as well, such as organic photodetectors.[59] Care should therefore be taken when employing these types of cross-coupling reactions and a next step might be the search for new catalyst systems that eliminate the formation of homocoupling entirely.

Acknowledgements

This work was supported by the Research Program of the Research Foundation – Flanders (FWO) (postdoctoral fellowships J.K. and P.V). M.K. and J.B. acknowledge the former

Agency for Innovation by Science and Technology in Flanders (IWT; now FWO-SB) for their PhD grants. The authors are also grateful to H. Penxten for the CV measurements.

Appendix A. Supplementary data

Supplementary data related to this article can be found at

References

[1] F.C. Krebs, T. Tromholt, M. Jorgensen, Upscaling of polymer solar cell fabrication using full roll-to-roll processing, Nanoscale 2 (6) (2010) 873−886.

[2] I. Ramirez, M. Causa, Y. Zhong, N. Banerji, M. Riede, Key tradeoffs limiting the performance of organic photovoltaics, Adv. Energy Mater. 8 (28) 2018 1703551.

[3] M. Kaltenbrunner, M.S. White, E.D. Głowacki, T. Sekitani, T. Someya, N.S. Sariciftci, S. Bauer, Ultrathin and lightweight organic solar cells with high flexibility, Nature Communications. 3 (2012) 770.

[4] S.B. Darling, F. You, The case for organic photovoltaics, RSC Adv. 3 (39) (2013) 17633-17648.

[5] K.A. Mazzio, C.K. Luscombe, The future of organic photovoltaics, Chem. Soc. Rev. 44 (1) (2015) 78-90.

[6] H. Kang, G. Kim, J. Kim, S. Kwon, H. Kim, K. Lee, Bulk-heterojunction organic solar cells: five core technologies for their commercialization, Adv. Mater. 28 (36) (2016) 7821-7861.

[7] S.D. Collins, N.A. Ran, M.C. Heiber, T.-Q. Nguyen, Small is powerful: recent progress in solution-processed small molecule solar cells, Adv. Energy Mater. 7 (10) (2017) 1602242.

[8] C. Liu, K. Wang, X. Hu, Y. Yang, C.-H. Hsu, W. Zhang, S. Xiao, X. Gong, Y. Cao, Molecular weight effect on the efficiency of polymer solar cells, ACS Appl. Mater. Interfaces 5 (22) (2013) 12163-12167.

[9] L. Lu, T. Zheng, T. Xu, D. Zhao, L. Yu, Mechanistic studies of effect of dispersity on the photovoltaic performance of PTB7 polymer solar cells, Chem. Mater. 27 (2) (2015) 537-543.

[10] H.K.H. Lee, Z. Li, I. Constantinou, F. So, S.W. Tsang, S.K. So, Batch-to-batch variation of polymeric photovoltaic materials: its origin and impacts on charge carrier transport and device performances, Adv. Energy Mater. 4 (16) (2014) 1400768.

[11] K.H. Hendriks, W. Li, G.H.L. Heintges, G.W.P. Van Pruissen, M.M. Wienk, R.A.J. Janssen, Homocoupling defects in diketopyrrolopyrrole-based copolymers and their effect on photovoltaic performance, J. Am. Chem. Soc. 136 (31) (2014) 11128-11133.

[12] T. Vangerven, P. Verstappen, J. Drijkoningen, W. Dierckx, S. Himmelberger, A. Salleo, D. Vanderzande, W. Maes, J.V. Manca, Molar mass versus polymer solar cell performance: highlighting the role of homocouplings, Chem. Mater. 27 (10) (2015) 3726–3732.

[13] F. Lombeck, H. Komber, D. Fazzi, D. Nava, J. Kuhlmann, D. Stegerer, K. Strassel, J. Brandt, A.D. de Zerio Mendaza, C. Müller, W. Thiel, M. Caironi, R. Friend, M. Sommer, Organic solar cells: on the effect of prevalent carbazole homocoupling defects on the photovoltaic performance of PCDTBT:$PC_{71}BM$ solar cells, Adv. Energy Mater. 6 (21) (2016) 1601232.

[14] G. Pirotte, J. Kesters, T. Cardeynaels, P. Verstappen, J. D'Haen, L. Lutsen, B. Champagne, D. Vanderzande, W. Maes, The impact of acceptor–acceptor homocoupling on the optoelectronic properties and photovoltaic performance of $PDTSQx_{ff}$ low bandgap polymers, Macromol. Rapid Commun. 39 (14) (2018) 1800086.

[15] G. Pirotte, P. Verstappen, D. Vanderzande, W. Maes, On the “true” structure of push–pull-type low-bandgap polymers for organic electronics, Adv. Electron. Mater. 4 (10) (2018) 1700481.

[16] P. Verstappen, I. Cardinaletti, T. Vangerven, W. Vanormelingen, F. Verstraeten, L. Lutsen, D. Vanderzande, J. Manca, W. Maes, Impact of structure and homo-coupling of the central donor unit of small molecule organic semiconductors on solar cell performance, RSC Adv. 6 (38) (2016) 32298–32307.

[17] T. Vangerven, P. Verstappen, N. Patil, J. D’Haen, I. Cardinaletti, J. Benduhn, N. Van den Brande, M. Defour, V. Lemaur, D. Beljonne, R. Lazzaroni, B. Champagne, K. Vandewal, J.W. Andreasen, P. Adriaensens, D.W. Breiby, B. Van Mele, D. Vanderzande, W. Maes, J. Manca, Elucidating batch-to-batch variation caused by homocoupled side products in solution-processable organic solar cells, Chem. Mater. 28 (24) (2016) 9088–9098.

[18] A. Yella, H.-W. Lee, H.N. Tsao, C. Yi, A.K. Chandiran, K. Nazeeruddin, E.W.-G. Diau, C.-Y. Yeh, S.M. Zakeeruddin, M. Grätzel, Porphyrin-sensitized solar cells with cobalt (II/III)-based redox electrolyte exceed 12 percent efficiency, Science. 334 (6056) (2011) 629-633.

[19] S. Mathew, A. Yella, P. Gao, R. Humphry-Baker, B.F.E. Curchod, N. Ashari-Astani, I. Tavernelli, U. Rothlisberger, K. Nazeeruddin, M. Grätzel, Dye-sensitized solar cells with 13% efficiency achieved through the molecular engineering of porphyrin sensitizers, Nat. Chem. 6 (2014) 242-247.

[20] J. Kesters, P. Verstappen, M. Kelchtermans, L. Lutsen, D. Vanderzande, W. Maes, Porphyrin-based bulk heterojunction organic photovoltaics: the rise of the colors of life, Adv. Energy Mater. 5 (13) (2015) 1500218.

[21] I. Obraztsov, W. Kutner, F. D’Souza, Evolution of molecular design of porphyrin chromophores for photovoltaic materials of superior light-to-electricity conversion efficiency, Sol. RRL 1 (2) (2017) 1600002.

[22] A. Mahmood, J.-Y. Hu, B. Xiao, A. Tang, X. Wang, E. Zhou, Recent progress in porphyrin-based materials for organic solar cells, J. Mater. Chem. A 6 (35) (2018) 16769-16797.

[23] K. Gao, J. Miao, L. Xiao, W. Deng, Y. Kan, T. Liang, C. Wang, F. Huang, J. Peng, Y. Cao, F. Liu, T.P. Russell, H. Wu, X. Peng, Multi-length-scale morphologies driven by mixed additives in porphyrin-based organic photovoltaics, Adv. Mater. 28 (23) (2016) 4727-4733.

[24] T. Liang, L. Xiao, K. Gao, W. Xu, X. Peng, Y. Cao, Modifying the chemical structure of a porphyrin small molecule with benzothiophene groups for the reproducible fabrication of high performance solar cells, ACS Appl. Mater. Interfaces 9 (8) (2017) 7131-7138.

[25] K. Ogumi, T. Nakagawa, H. Okada, R. Sakai, H. Wang, Y. Matsuo, Substituent effects in magnesium tetraethynylporphyrin with two diketopyrrolopyrrole units for bulk heterojunction organic solar cells, J. Mater. Chem. A 5 (44) (2017) 23067-23077.

[26] M. Vartanian, R. Singhal, P. de la Cruz, S. Biswas, G.D. Sharma, F. Langa, Low energy loss of 0.57 eV and high efficiency of 8.80% in porphyrin-based BHJ solar cells, ACS Appl. Mater. Interfaces 1 (3) (2018) 1304-1315.

[27] K. Gao, L. Li, T. Lai, L. Xiao, Y. Huang, F. Huang, J. Peng, Y. Cao, F. Liu, T.P. Russell, R.A.J. Janssen, X. Peng, Deep absorbing porphyrin small molecule for high-performance organic solar cells with very low energy losses, J. Am. Chem. Soc. 137 (23) (2015) 7282-7285.

[28] M. Vartanian, P. de la Cruz, S. Biswas, G.D. Sharma, F. Langa, Panchromatic ternary organic solar cells with 9.44% efficiency incorporating porphyrin-based donors, Nanoscale 10 (25) (2018) 12100-12108.

[29] A. Zhang, C. Li, F. Yang, J. Zhang, Z. Wang, Z. Wei, W. Li, An electron acceptor with porphyrin and perylene bisimides for efficient non-fullerene solar cells, Angew. Chem. Int. Ed. 56 (10) (2017) 2694-2698.

[30] J. Hou, O. Inganäs, R.H. Friend, F. Gao, Organic solar cells based on non-fullerene acceptors, Nature Materials 17 (2018) 119-128.

[31] C. Yan, S. Barlow, Z. Wang, H. Yan, A.K.Y. Jen, S.R. Marder, X. Zhan, Non-fullerene acceptors for organic solar cells, Nature Reviews Materials 3 (2018) 18003.

[32] S. Li, L. Ye, W. Zhao, H. Yan, B. Yang, D. Liu, W. Li, H. Ade, J. Hou, A wide band gap polymer with a deep highest occupied molecular orbital level enables 14.2% efficiency in polymer solar cells, J. Am. Chem. Soc. 140 (23) (2018) 7159-7167.

[33] L. Meng, Y. Zhang, X. Wan, C. Li, X. Zhang, Y. Wang, X. Ke, Z. Xiao, L. Ding, R. Xia, H.-L. Yip, Y. Cao, Y. Chen, Organic and solution-processed tandem solar cells with 17.3% efficiency, Science 361 (6407) (2018) 1094-1098.

[34] H. Qin, L. Li, F. Guo, S. Su, J. Peng, Y. Cao, X. Peng, Solution-processed bulk heterojunction solar cells based on a porphyrin small molecule with 7% power conversion efficiency, Energy Environ. Sci. 7 (4) (2014) 1397-1401.

[35] Y. Liu, J. Zhao, Z. Li, C. Mu, W. Ma, H. Hu, K. Jiang, H. Lin, H. Ade, H. Yan, Aggregation and morphology control enables multiple cases of high-efficiency polymer solar cells, Nature communications 5 (2014) 5293.

[36] T. Bessho, S.M. Zakeeruddin, C.-Y. Yeh, E.W.-G. Diau, M. Grätzel, Highly efficient mesoscopic dye-sensitized solar cells based on donor–acceptor-substituted porphyrins, Angew. Chem. Int. Ed. 49 (37) (2010) 6646-6649.

[37] D. Popović, I. Ata, J. Krantz, S. Lucas, M. Lindén, E. Mena-Osteritz, P. Bäuerle, Preparation of efficient oligomer-based bulk-heterojunction solar cells from eco-friendly solvents, J. Mater. Chem. C 5 (38) (2017) 9920-9928.

[38] S. Li, L. Ye, W. Zhao, S. Zhang, S. Mukherjee, H. Ade, J. Hou, Energy-level modulation of small-molecule electron acceptors to achieve over 12% efficiency in polymer solar cells, Adv. Mater. 28 (42) (2016) 9423-9429.

[39] W. Vanormelingen, J. Kesters, P. Verstappen, J. Drijkoningen, J. Kudrjasova, S. Koudjina, V. Liégeois, B. Champagne, J. Manca, L. Lutsen, D. Vanderzande, W. Maes, Enhanced open-circuit voltage in polymer solar cells by dithieno[3,2-b:2′,3′-d]pyrrole N-acylation, J. Mater. Chem. A 2 (20) (2014) 7535–7545.

[40] S. Belanger, M.H. Keefe, J.L. Welch, J.T. Hupp, Rapid derivatization of mesoporous thin-film materials based on Re(I) zinc-porphyrin 'molecular squares': selective modification of mesopore size and shape by binding of aromatic nitrogen donor ligands, Coord. Chem. Rev. 192 (1999) 29-45.

[41] J. D. Zimmerman, E.K. Yu, V.V. Diev, K. Hanson, M.E. Thompson, S.R. Forrest, Use of additives in porphyrin-tape/C60 near-infrared photodetectors, Org. Electron. 12 (5) (2011) 869-873.

[42] S.H. Kang, I.T. Choi, M.S. Kang, Y.K. Eom, M.J. Ju, J.Y. Hong, H.S. Kangb, H.K. Kim, Novel D–π–A structured porphyrin dyes with diphenylamine derived electron-donating substituents for highly efficient dye-sensitized solar cells, J. Mater. Chem. A 1 (12) (2013) 3977-3982.

[43] J. Huber, C. Jung, S. Mecking, Nanoparticles of low optical band gap conjugated polymers, Macromolecules 45 (19) (2012) 7799-7805.

[44] D. Kotowski, S. Luzzati, G. Bianchi, A. Calabrese, A. Pellegrino, R. Po, G. Schimperna, A. Tacca, Double acceptor D–A copolymers containing benzotriazole and benzothiadiazole units: chemical tailoring towards efficient photovoltaic properties, J. Mater. Chem. A 1 (36) (2013) 10736-10744.

[45] S. Hiroto, Y. Miyake, H. Shinokubo, Synthesis and functionalization of porphyrins through organometallic methodologies, Chem. Rev. 117 (4) (2017) 2910−3043.

[46] H.L. Anderson, S.J. Martin, D.D.C. Bradley, Synthesis and third-order nonlinear optical properties of a conjugated porphyrin polymer, Angew. Chem. Int. Ed. Engl. 33 (6) (1994) 655−657.

[47] A. Kato, K. Sugiura, H. Miyasaka, H. Tanaka, T. Kawai, M. Sugimoto, M.A. Yamashita, A square cyclic porphyrin dodecamer: synthesis and single-molecule characterization, Chem. Lett. 33 (5) (2004) 578−579.

[48] W.J. Youngblood, D.T. Gryko, R.K. Lammi, D.F. Bocian, D. Holten, J.S. Lindsey, Glaser-mediated synthesis and photophysical characterization of diphenylbutadiyne-linked porphyrin dyads, J. Org. Chem. 67 (7) (2002) 2111−2117.

[49] R. Mishra, R. Regar, R. Singhal, P. Panini, G.D. Sharma, J. Sankar, Porphyrin based push–pull conjugates as donors for solution-processed bulk heterojunction solar cells: a case of metal-dependent power conversion efficiency, J. Mater. Chem. A 5 (30) (2017) 15529-15533.

[50] T. Lai, X. Chen, L. Xiao, L. Zhang, T. Liang, X. Peng, Y. Cao, Conjugated D−A porphyrin dimers for solution-processed bulk-heterojunction organic solar cells, Chem. Commun. 53 (2017) 5113-5116.

[51] Y. Huang, L. Li, X. Peng, J. Peng, Y. Cao, Solution processed small molecule bulk heterojunction organic photovoltaics based on a conjugated donor–acceptor porphyrin, J. Mater. Chem. 22 (41) (2012) 21841-21844.

[52] K. Gao, L. Xiao, Y. Kan, B. Yang, J. Peng, Y. Cao, F. Liu, T. Russell, X. Peng, Solution-processed bulk heterojunction solar cells based on porphyrin small molecules with very low energy losses comparable to perovskite solar cells and high quantum efficiencies, J. Mater. Chem. C 4 (17) (2016) 3843-3850.

[53] H. Wang, L. Xiao, L. Yan, S. Chen, X. Zhu, X. Peng, X. Wang, W.-K. Wong and W.-Y. Wong, Structural engineering of porphyrin-based small molecules as donors for efficient organic solar cells, Chem. Sci. 7 (7) (2016) 4301-4307.

[54] L. Li, Y. Huang, J. Peng, Y. Cao, X. Peng, Enhanced performance of solution-processed solar cells based on porphyrin small molecules with a diketopyrrolopyrrole acceptor unit and a pyridine additive, J. Mater. Chem. A 1 (6) (2013) 2144-2150.

[55] K. Vandewal, J. Widmer, T. Heumueller, C.J. Brabec, M.D. McGehee, K. Leo, M. Riede, A. Salleo, Increased open-circuit voltage of organic solar cells by reduced donor-acceptor interface area, Adv. Mater. 26 (23) (2014) 3839-3843.

[56] D. Veldman, O. Ipek, S.C.J. Meskers, J. Sweelssen, M.M. Koetse, S.C. Veenstra, J.M. Kroon, S.S. van Bavel, J. Loos, R.A.J. Janssen, Compositional and electric field dependence of the dissociation of charge transfer excitons in alternating polyfluorene copolymer/fullerene blends, J. Am. Chem. Soc. 130 (24) (2008) 7721–7735.

[57] Z. Yi, W. Ni, Q. Zhang, M. Li, B. Kan, X. Wan, Y. Chen, Effect of thermal annealing on active layer morphology and performance for small molecule bulk heterojunction organic solar cells, J. Mater. Chem. C 2 (35) (2014) 7247–7255.

[58] K. Vandewal, A. Gadisa, W.D. Oosterbaan, S. Bertho, F. Banishoeib, I. Van Severen, L. Lutsen, T.J. Cleij, D. Vanderzande, J.V. Manca, The relation between open-circuit voltage and the onset of photocurrent generation by charge-transfer absorption in polymer : fullerene bulk heterojunction solar cells, Adv. Funct. Mater. 18 (14) (2008) 2064-2070.

[59] L. Li, Y. Huang, J. Peng, Y. Cao, X. Peng, Highly responsive organic near-infrared photodetectors based on a porphyrin small molecule, J. Mater. Chem. C 2 (8) (2014) 1372-1375.

HIGHLIGHTS

- Efforts to increase our understanding of the effect of homocoupling on photovoltaic performance are presented
- D-A-π-A-D conjugated chromophores based on an A_2B_2-*meso*-ethynylporphyrin core are synthesized
- Power conversion efficiencies up to 4.6% are achieved
- The presence of (Glaser type) homocoupled side products mainly reduces the open-circuit voltage and fill factor